How to cite: *Angew. Chem. Int. Ed.* **2022,** *61,* e202201101
International Edition: doi.org/10.1002/anie.202201101
German Edition: doi.org/10.1002/ange.202201101

Nanozymes

A Valence-Engineered Self-Cascading Antioxidant Nanozyme for the Therapy of Inflammatory Bowel Disease

*Quan Wang, Chaoqun Cheng, Sheng Zhao, Quanyi Liu, Yihong Zhang, Wanling Liu, Xiaozhi Zhao, He Zhang, Jun Pu, Shuo Zhang, Huigang Zhang, Yan Du, and Hui Wei**

Abstract: Antioxidant treatment strategy by scavenging reactive oxygen species (ROS) is a highly effective disease treatment option. Nanozymes with multiple antioxidant activities can cope with the diverse ROS environment. However, lack of design strategies and limitation of negative correlation for nanozymes with multiple antioxidant activities hindered their development. To overcome these difficulties, here we used $ZnMn_2O_4$ as a model to explore the role of Mn valency at the octahedral site via a valence-engineered strategy, and found that its multiple antioxidant activities are positively correlated with the content of Mn^{4+}. Therefore, through this strategy, a self-cascading antioxidant nanozyme $LiMn_2O_4$ was constructed, and its efficacy was verified at the cellular level and in an inflammatory bowel disease model. This work not only provides guidance for the design of multiple antioxidant nanozymes, but also broadens the biomedical application potential of multiple antioxidant nanozymes.

Introduction

Reactive oxygen species (ROS) are involved in many biological phenomena and play an important role in regulating the various physiological functions of organisms.[1] However, excessive production of ROS can cause oxidative stress in the organisms and lead to the occurrence of diseases.[2] The ROS produced in organisms can be scavenged by antioxidant enzymes, such as superoxide dismutase (SOD), catalase (CAT), and glutathione peroxidase (GPx). Under pathological conditions, these enzymes are not enough to scavenge overproduced ROS. Therefore, it is necessary to develop more effective therapy strategies to treat ROS-related diseases by exploring artificial enzymes with the activities of antioxidant enzymes.[3]

As an emerging type of artificial enzymes, nanozymes have broad research prospects because of their simple preparation, high stability, designability, wide sources, and potential for large-scale production.[4] Particularly, antioxidant nanozymes have been explored for various disease therapies.[5] Unfortunately, a nanozyme with a single enzyme-like activity is not enough to effectively scavenge excessive ROS in the complex pathological environments. While nanozymes with multiple enzyme-like activities have been developed to tackle this issue, most of nanozymes do not exhibit the best of these multi-activities simultaneously. For example, the SOD- and the CAT-like activities of cerium oxide are negatively correlated (i.e., a higher ratio of Ce^{3+}/Ce^{4+} leads to a better SOD-like activity while a higher ratio of Ce^{4+}/Ce^{3+} leads to a better CAT-like activity).[6] Currently, the design and mechanistic exploration of nanozymes with simultaneous multiple antioxidant activities is quite challenging. To address this challenge, herein, we report a valence-engineered strategy to develop self-cascading nanozymes with simultaneous multiple antioxidant activities.

[*] Q. Wang, C. Cheng, Dr. S. Zhao, Y. Zhang, W. Liu, S. Zhang, Dr. H. Zhang, Dr. H. Wei
College of Engineering and Applied Sciences, Nanjing National Laboratory of Microstructures, Jiangsu Key Laboratory of Artificial Functional Materials, Nanjing University
Nanjing, Jiangsu 210023 (China)
E-mail: weihui@nju.edu.cn

Q. Liu, Dr. Y. Du
State Key Laboratory of Electroanalytical Chemistry, Changchun Institute of Applied Chemistry, Chinese Academy of Sciences
Changchun, Jilin 130022 (China)

Q. Liu, Dr. Y. Du
University of Science and Technology of China
Hefei, Anhui 230026 (China)

Dr. X. Zhao
Department of Urology, Drum Tower Hospital, Medical School of Nanjing University, Institute of Urology, Nanjing University
Nanjing, Jiangsu 210008 (China)

Dr. H. Zhang
Department of Periodontology, Nanjing Stomatological Hospital, Medical School of Nanjing University
Nanjing, Jiangsu 210093 (China)

Dr. J. Pu
Key Laboratory of Functional Molecular Solids, Ministry of Education, College of Chemistry and Materials Science,
Anhui Normal University
Wuhu 241002 (China)

S. Zhang, Dr. H. Zhang
Collaborative Innovation Center of Advanced Microstructures and Institute of Materials Engineering, Nanjing University
Nanjing, Jiangsu 210093 (China)

Dr. H. Wei
State Key Laboratory of Analytical Chemistry for Life Science, School of Chemistry and Chemical Engineering, Chemistry and Biomedicine Innovation Center (ChemBIC), Nanjing University
Nanjing, Jiangsu 210023 (China)

It is worth noting that when the multiple antioxidant activities of a nanozyme are positively correlated, it easily forms a cascade reaction. The cascade reaction greatly improves the catalytic efficiency because of its high local reactant concentration, reduced intermediate decomposition and high mass transfer efficiency.[7] To this end, such a nanozyme can achieve more significant therapeutic efficacy in the treatment of diseases and may even reduce the administration dosage. Because of the above-mentioned limitations of available nanozymes with multiple antioxidant activities, the current cascade nanozymes are mainly constructed by two or more materials,[8] which require delicate material design and complicated material synthesis. These requirements can be satisfied by developing self-cascading antioxidant nanozymes with simultaneous multi-activities.[9]

In this work, we used spinel oxide $ZnMn_2O_4$ (where Zn occupies tetrahedral sites and Mn occupies octahedral sites) as a model material to explore the effect of Mn valency at octahedral sites on its multiple antioxidant activities of nanozyme (Figure 1).[10] The Zn element is selected here because, on the one hand, Zn element is tetrahedral site-preferred and the valence state is stable; on the other hand, Zn is an important trace element in the human body. We chose to modulate the octahedral sites because they are dominant active sites, as demonstrated in previous studies.[11] Our results showed that $ZnMn_2O_4$ (named as ZM) only had a SOD-like activity (single antioxidant activity). As the valency of Mn increases from +3 to +4 by gradual Li doping, not only was the SOD-like activity of nanozyme improved, but also nanozyme exhibited gradually increased CAT-like and GPx-like activities. The finally optimized nanozyme $LiMn_2O_4$ (named as LM) achieved the best SOD-, CAT-, and GPx-like activities simultaneously, and had hydroxyl radical scavenging ability. The obtained LM exhibited good antioxidant and therapeutic effects at the cellular level and in an inflammatory bowel disease (IBD) model.[12] Notably, LM showed obvious dosage advantages in animal experiments. These results have significant guiding

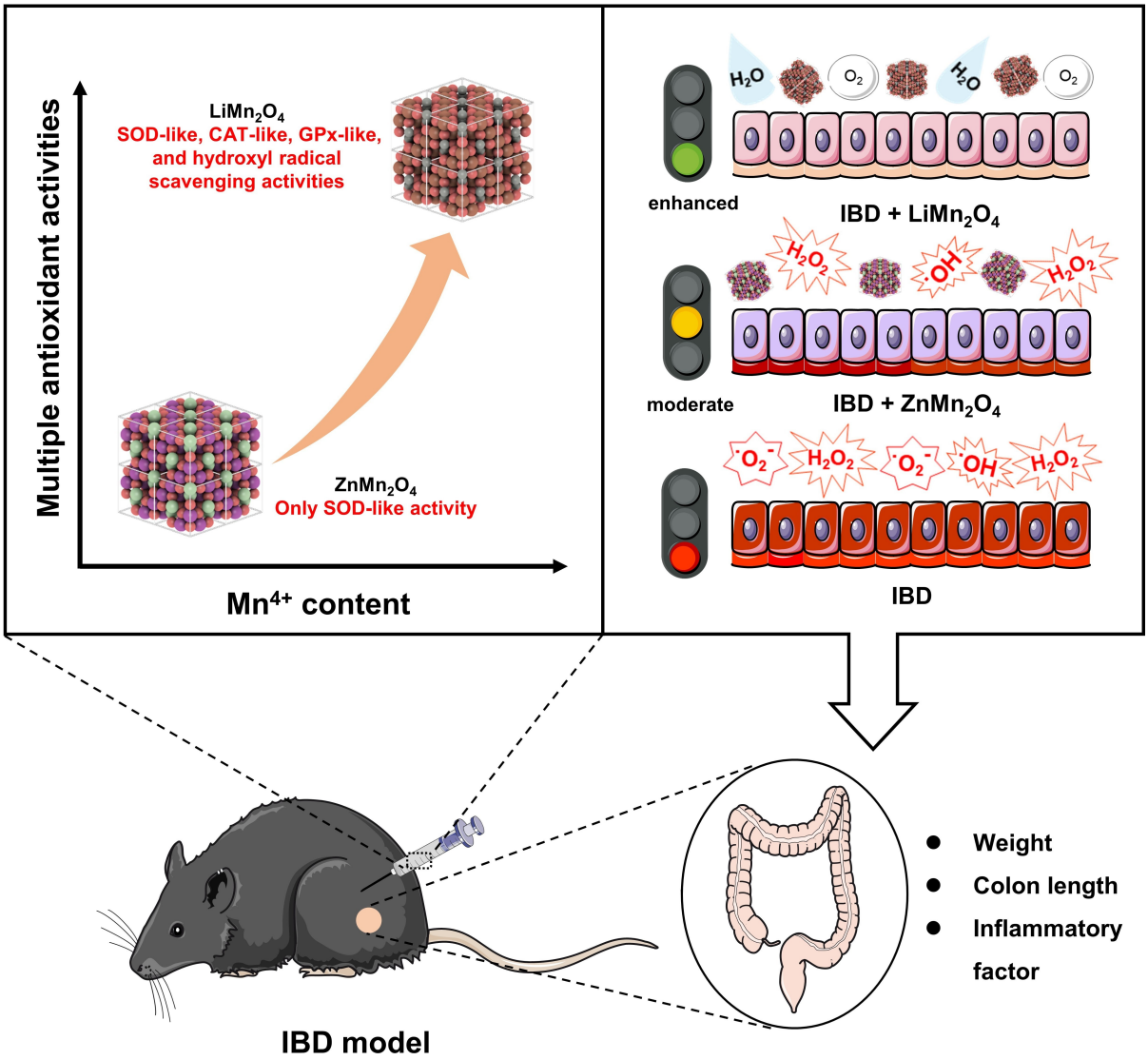

Figure 1. Valence-engineering of manganese spinel oxide to design self-cascading antioxidant nanozymes for enhanced IBD therapy.

for the design and development of nanozymes with simultaneous multiple antioxidant activities.

Results and Discussion

Design, Synthesis, and Characterization of $Zn_{1-x}Li_xMn_2O_4$ ($x = 0$, 0.2, 0.4, 0.6, 0.8, and 1) and $LiMn_2O_4$

The general form of spinel oxide is AB_2O_4, where A occupies one tetrahedral site and B occupies two octahedral sites. We chose $ZnMn_2O_4$ as the initial model material, and adjusted the valence state of Mn by doping Li. Here, Zn and Li, as elements with stable valence states, are not the key factors affecting catalytic activity and are both essential trace elements for the human body.

A series of Li-doped samples $Zn_{1-x}Li_xMn_2O_4$ ($x = 0$, 0.2, 0.4, 0.6, 0.8, and 1) were synthesized by a hydrothermal method with nitrate metal salts as the precursors. The obtained products were named as ZM, Li-2, Li-4, Li-6, Li-8, and Li-10. Please refer to the experimental section for synthesis details. The XRD results showed that ZM, Li-2, Li-4, and Li-6 all maintained the phase of $ZnMn_2O_4$, and there was no obvious impurity peak, which indicated the successful incorporation of Li element and the formation of solid solutions (Figure S1b). However, Li-8 and Li-10 showed both $ZnMn_2O_4$ and $LiMn_2O_4$ phases, which mean that it is difficult to synthesize a pure $LiMn_2O_4$ phase with nitrate as the precursor (Figure S2). As a comparison sample for the most Li doping, we used potassium permanganate ($KMnO_4$) as the precursor to synthesize $LiMn_2O_4$ (named as LM). The successful synthesis of LM was confirmed by XRD (Figure S1a). The amount of Li doped in $Zn_{1-x}Li_xMn_2O_4$ was measured by an inductively coupled plasma (ICP) instrument (Table S1). The actual Li content was lower than the stoichiometric ratio. This revealed the limited extent of Li doping in this method and also verified the XRD results. TEM results indicated that these samples (ZM, Li-2, Li-4, Li-6, and LM) were all irregular nanoparticles with similar sizes around 20 nm (Figure S1c), which excluded the extra influence of special morphology on enzyme-like activity. The Brunauer–Emmett–Teller (BET) surface area measurements showed similar results (Figure S1d) and the specific data are listed in Table S2. All these results confirmed the successful preparation of ZM, Li-2, Li-4, Li-6, and LM.

The size and charge of the materials have been characterized using DLS (Figure S3). The particle size of these materials was around 100 nm (Figure S3a). The results of zeta potential showed an interesting phenomenon. As the Li doping amount increased, the charge shifted from positive to negative (Figure S3b). Negatively charged nanoparticles are favorable for binding to the lesion site (usually positively charged).[13]

Multiple Antioxidant Activity Measurement of ZM, Li-2, Li-4, Li-6, and LM

To investigate the simultaneous multiple antioxidant capabilities of ZM, Li-2, Li-4, Li-6, and LM, various types of enzyme-like activities were tested. Because of the strong dependence of catalytic activities on the surface area of nanozymes, it is necessary to exclude the influence of the surface area. Here we used the normalized BET surface area to calculate and compare specific activities. Please refer to the experimental section for calculation details.

Scavenging of superoxide radicals is the initial step of the antioxidant cascade. With the incorporation of Li, the SOD-like activity of nanozymes gradually increased, and the trend was ZM < Li-2 < Li-4 < Li-6 < LM (Figure 2a and Figure S4). Compared with ZM, the SOD-like activity of LM had been nearly doubled. The hydrogen peroxide decomposition is the second step of the antioxidant cascade, and both CAT-like and GPx-like activities can achieve this effect. A similar activity trend was also obtained for the CAT-like and GPx-like activities of nanozymes (Figure S5, Figure S6, Figure 2b, and Figure 2c). It is worth noting that the initial model material ZM and the low-doped sample Li-2 hardly show CAT-like and GPx-like activities (their test results are negative). When a sufficient amount of Li was doped, the nanozyme (especially LM) exhibited obvious CAT-like and GPx-like activities. These results indicated that the Li doping strategy was an effective way to simultaneously regulate the multiple activities of nanozymes.

Furthermore, we conducted electron paramagnetic resonance (EPR) experiments to monitor the free radical scavenging ability of nanozymes. ZM and LM were chosen as the initial model material and the optimized material for comparison, respectively. In terms of superoxide radical elimination performance (Figure 2d), LM showed significantly higher activity and dosage advantages. The competition reaction of nanozyme and Fe^{2+} combined with H_2O_2 was adopted to investigate the effect of nanozyme on decomposing H_2O_2. There was no change in the peak intensity of hydroxyl radicals, indicating that ZM itself does not have the ability to decompose H_2O_2. In contrast, the H_2O_2 decomposing ability of LM showed a clear concentration dependence (Figure 2e). In addition to ROS, the reactive nitrogen species (RNS) and hydroxyl radical scavenging capabilities of these nanozymes were examined. Li-2, Li-4, and LM showed obvious hydroxyl radical scavenging ability (LM also achieved the best activity), while ZM and Li-6 had negligible scavenging ability (Figure S7a). The results of EPR also verified the same conclusion (Figure S7b). This trend was different from the above-mentioned enzyme-like activities. $DPPH^{\bullet}$ and $ABTS^{+\bullet}$ as typical RNS were used to study the nanozymes' RNS scavenging activity. It showed that ZM, Li-2, Li-4, Li-6, and LM did not reflect the scavenging activity and concentration dependence (Figure S8 and Figure S9). In short, based on the above study of SOD-like, CAT-like, and GPx-like activities, the optimized LM achieved self-cascading antiox-

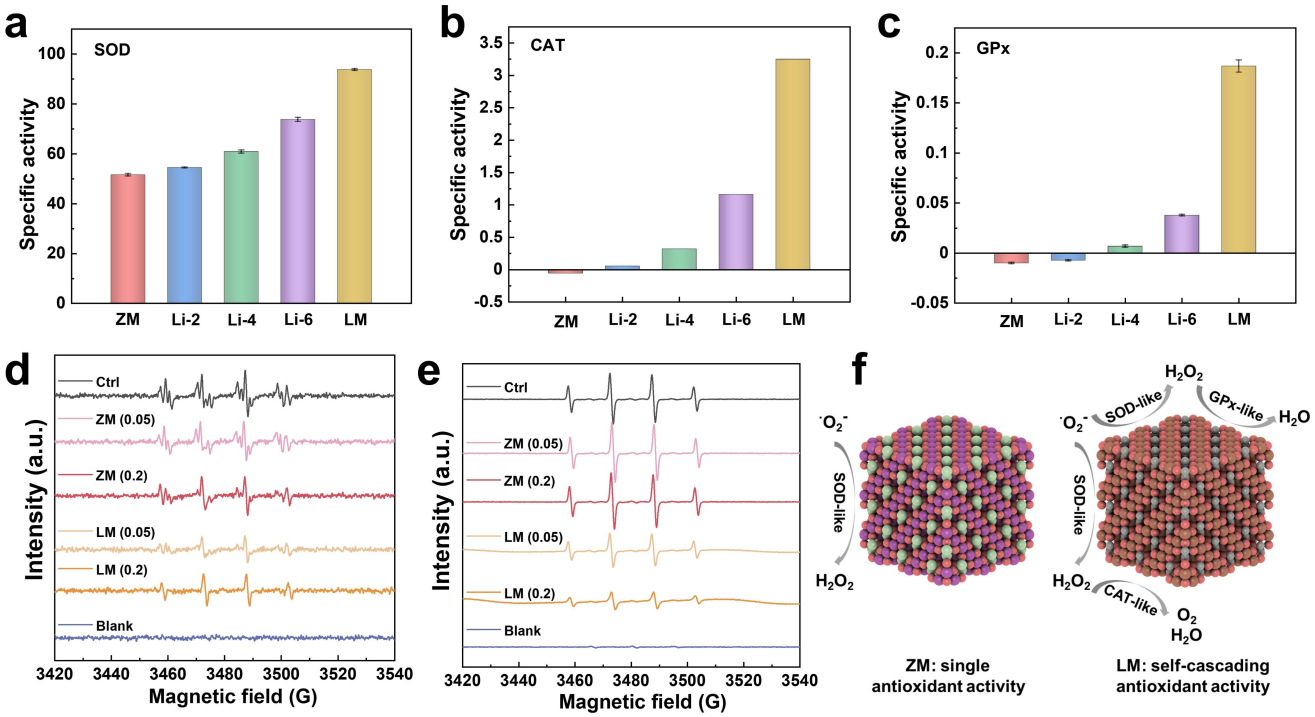

Figure 2. Antioxidant activity of ZM, Li-2, Li-4, Li-6, and LM. a) SOD-like b) CAT-like and c) GPx-like specific activities of ZM, Li-2, Li-4, Li-6, and LM. EPR for elimination of d) $^{\bullet}O_2^-$ and e) H_2O_2. 0.05 and 0.2 in parentheses refer to 0.05 mg mL^{-1} and 0.2 mg mL^{-1} nanozymes, respectively. f) Comparison of antioxidant activity before and after valence engineering.

idant activity, while the original material ZM only had a single antioxidant activity (Figure 2f).

Multiple Antioxidant Activities Regulated by Valence-Engineered Strategy

The catalytic process is generally carried out on the surface of the nanomaterials. Therefore, to reveal the key factor underlying the multiple antioxidant activities of nanozymes, we carried out the measurement of X-ray photoelectron spectroscopy (XPS) to investigate the surface properties of nanozymes. The full XPS spectra of ZM, Li-2, Li-4, Li-6, and LM were shown in Figure S10a. Zn, Mn, and O elements were clearly detected. Notably, the peak of Li 1*s* was so weak that it was covered by the peak of Mn 3*p*. This is attributed to the low content of Li element and the light weight of Li atom (Figure S10b). The spectral deconvolution was performed to O 1*s* and Zn 2*p* as shown in Figure S11. For all samples, the peak positions of Zn 2*p* were nearly the same, indicating that Zn is not a key factor affecting the activity. The peak positions of O 1*s* were all around 530.0 eV, and the content of O_β increased slightly during doping and then decreased, which implied that a small amount of metal ion vacancies were generated during the doping process (Figure S11a). However, the change of O_β did not show an obvious correlation with the enzyme-like catalytic activity, which means that the O_β content is not a key factor affecting the activity.

Interestingly, the peak positions of Mn 2*p* ($2p_{1/2}$ and $2p_{3/2}$) shifted to the high-energy region with the increase of Li doping amount, which indicated a decrease in covalency (Figure 3a). The results of fitting peaks showed that the contents of Mn^{4+} (red line) and Mn^{3+} (blue line) have changed significantly.[14] The molar ratio of Mn^{4+}/Mn^{3+} increased from 0.56 for the initial ZM to 2.29 for the final LM. Accordingly, the average valence of Mn increased from 3.36 for ZM to 3.70 for LM (Figure 3b). This revealed that the Li doping strategy is essentially a valence-engineered strategy. By plotting the multiple antioxidant activities as a function of the Mn^{4+} content (that is, the valence state of Mn), and a positive correlation was obtained. When we increased the content of Mn^{4+}, all the antioxidant activities of the model material have been improved (Figure 3c). This is probably the first example that the multiple antioxidant activities of nanozymes are enhanced simultaneously.

Furthermore, we studied the CAT-like activity of in a 150 mL PBS buffer solution (pH 7.4, 0.01 M) containing 30 mg LM and 5 mM H_2O_2. Then collected LM after the reaction for XRD and XPS analysis to investigate the reaction stability of the material and the potential valence state change after the reaction. The XRD result (Figure S12) showed that the material collected after the reaction still maintained good crystallinity. In addition, some new weak peaks could be assigned to the buffer salt and the divalent manganese compound formed after the partial degradation of the material.[15] We also calculated the material recovery rate, which was greater than 96 %. The peak fitting results of Mn 2*p* were similar to those before the reaction, and the

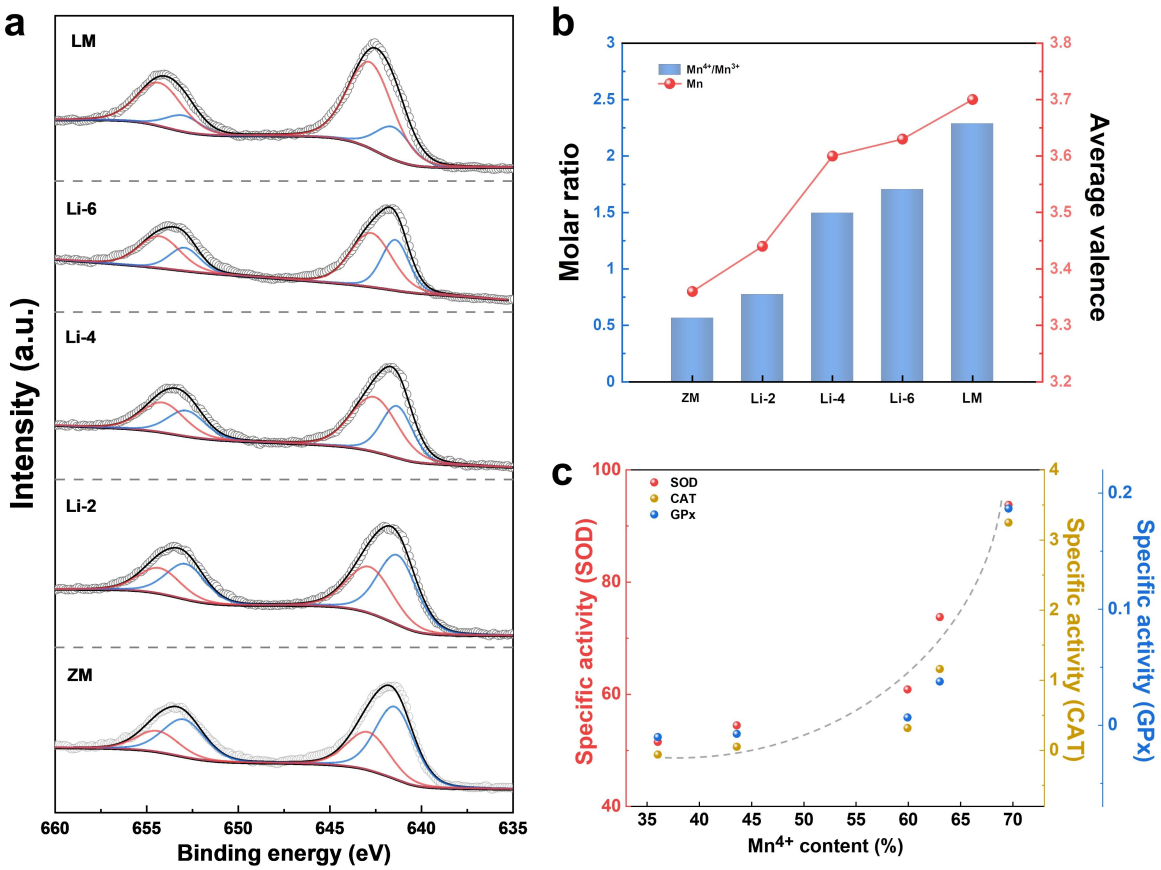

Figure 3. Antioxidant nanozyme optimized based on Mn valence. a) Mn 2*p* of ZM, Li-2, Li-4, Li-6, and LM. The red and blue lines represent the peaks of Mn^{4+} and Mn^{3+}, respectively. b) Mn^{4+}/Mn^{3+} molar ratio and the average valence of Mn of ZM, Li-2, Li-4, Li-6, and LM obtained by XPS-peak-deconvolution. c) Relationship between Mn^{4+} content and antioxidant activity (the gray line is shown for eye-guiding only).

tetravalent manganese still maintained the highest proportion (Figure S13b). The average valence state was 3.74, and there was no significant change (3.70 before the reaction). The XPS full spectra contained the peak of P 2*p* (Figure S13a). In addition, the fitting result of Mn 2*p* showed that it contained Mn^{2+} (satellite peaks) (Figure S13b), which also indicated the presence of a small amount of buffer salts and decomposed products, which corroborated the result of XRD. Collectively, these results demonstrated that the materials in this work exhibited more prominent catalytic properties.

Cellular Evaluation of ZM and LM

In view of the success of the valence-engineering strategy in regulating the multiple antioxidant activities of nanozymes, it is meaningful to explore the advantages of the optimized nanozyme (i.e., LM) in biomedical applications. In the following experiments, ZM was used as a comparison. Using CT26 cell line and Cell Counting Kit-8 (CCK-8) assay, the cytotoxicity of ZM and LM was evaluated. The cytotoxicity evaluation revealed that LM only exhibited toxicity when the concentration was greater than 100 $\mu g\,mL^{-1}$, which implied the good biocompatibility of LM (Figure 4a). ZM showed slightly better biocompatibility than LM, which may be benefited from the better water dispersibility of ZM (Figure 4b). Moreover, we carried out a study on the stability of the material. Specifically, LM (0.04 $mg\,mL^{-1}$) was incubated with PBS buffer solution (pH 7.4, 0.01 M) for 4 days to simulate the stability of the material in a physiological environment, and the leaching ratio of the metal ion was detected by ICP (Table S3). The leaching ratio of Li rapidly reached a plateau and was significantly higher than that of Mn, indicating a rapid exchange process with cations (such as Na) in solution (Figure S14a). The leaching ratio of Mn was between 2 % and 8 % with a slow upward trend over a period of 4 days, indicating the satisfactory stability of the material (Figure S14b).

Furthermore, the RAW264.7 cells were treated with H_2O_2 to simulate the overproduction of intracellular ROS and DCFH-DA was used as the fluorescence probe to monitor the cellular level of ROS. DCFH-DA can be converted to DCF after reacting with ROS. The results of flow cytometry showed that LM has excellent ROS scavenging ability, while the ability of ZM to eliminate intracellular ROS was weaker and did not show obvious concentration dependence (Figure 4c). The observation of laser scanning confocal microscopy clearly confirmed that compared with ZM, LM exhibited a better ability to eliminate intracellular

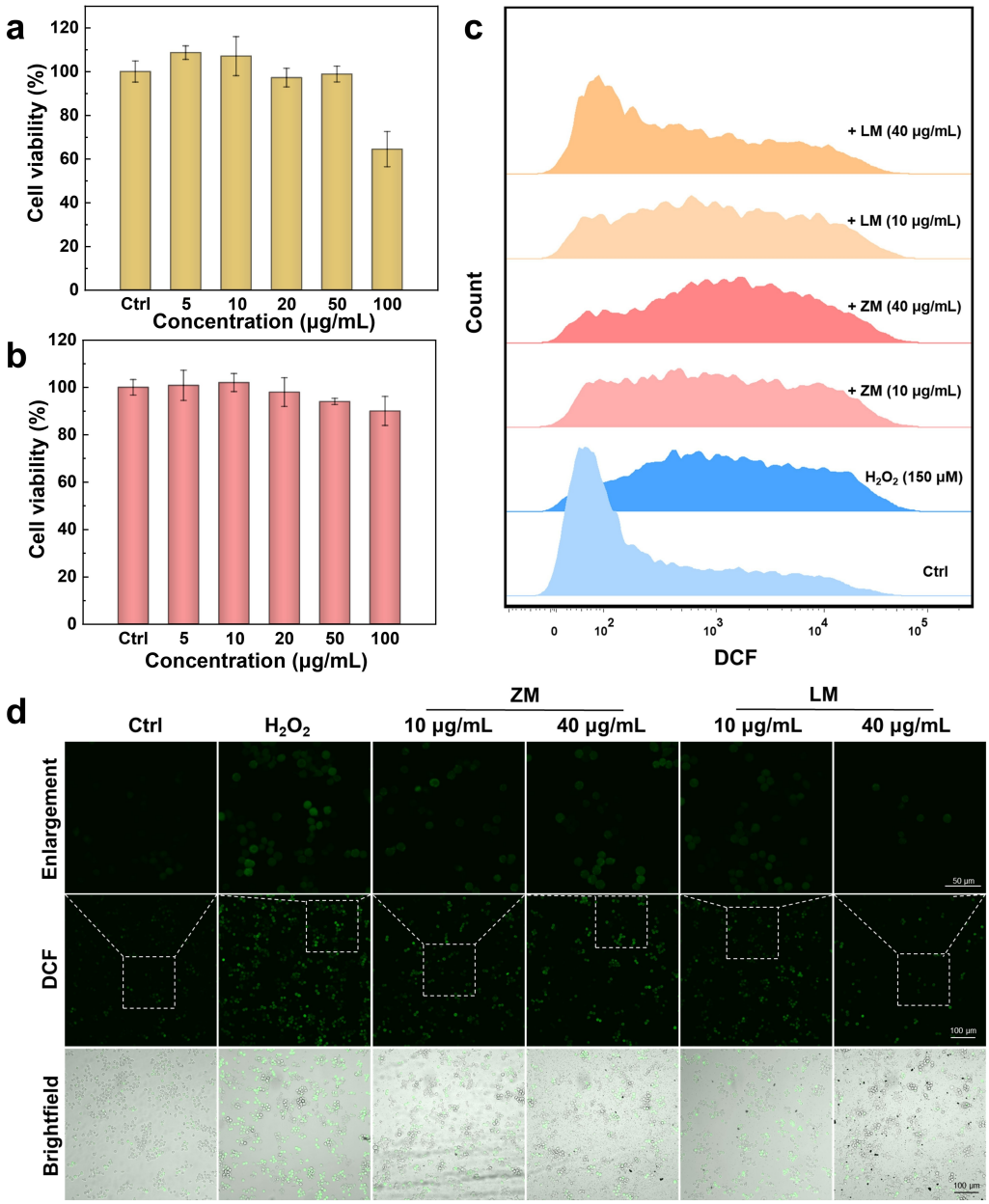

Figure 4. Cellular evaluation of ZM and LM. The cytotoxicity of a) LM and b) ZM by using CT26 cell line as a model. The ROS level of RAW264.7 cells monitored by c) a flow cytometer and d) a laser scanning confocal microscopy in the presence or absence of nanozymes. Scale bar in DCF and brightfield was 100 μm, and scale bar in enlargement was 50 μm.

ROS, especially at a dose of 40 $\mu g\,mL^{-1}$ (Figure 4d). Also, specific dyes have been used to investigate the regulation of ROS levels by nanozymes in cells. Specifically, dihydroethidium (DHE), ROSGreen and hydroxyphenyl fluorescein (HPF) are probes that specific for superoxide radicals, hydrogen peroxide and hydroxyl radicals, respectively. The results showed that LM could significantly mediate the levels of superoxide radicals, hydrogen peroxide and hydroxyl radicals in cells in a concentration-dependent manner (Figure S15). These results of cellular experiments proved that nanozymes with simultaneous multiple antioxidant activities are more powerful to scavenge overproduced ROS in organisms. To this end, LM with the best multiple enzyme-like activities should have great promise in biomedical applications.

In Vivo Anti-Inflammation Therapy

Based on the excellent multiple antioxidant activity and good biocompatibility of LM, its ability to treat diseases such as inflammation was investigated in a mouse model of dextran sulfate sodium (DSS)-induced inflammatory bowel disease (IBD). IBD is an inflammatory disease accompanied by excessive production of ROS. ZM and 5-aminosalicylic

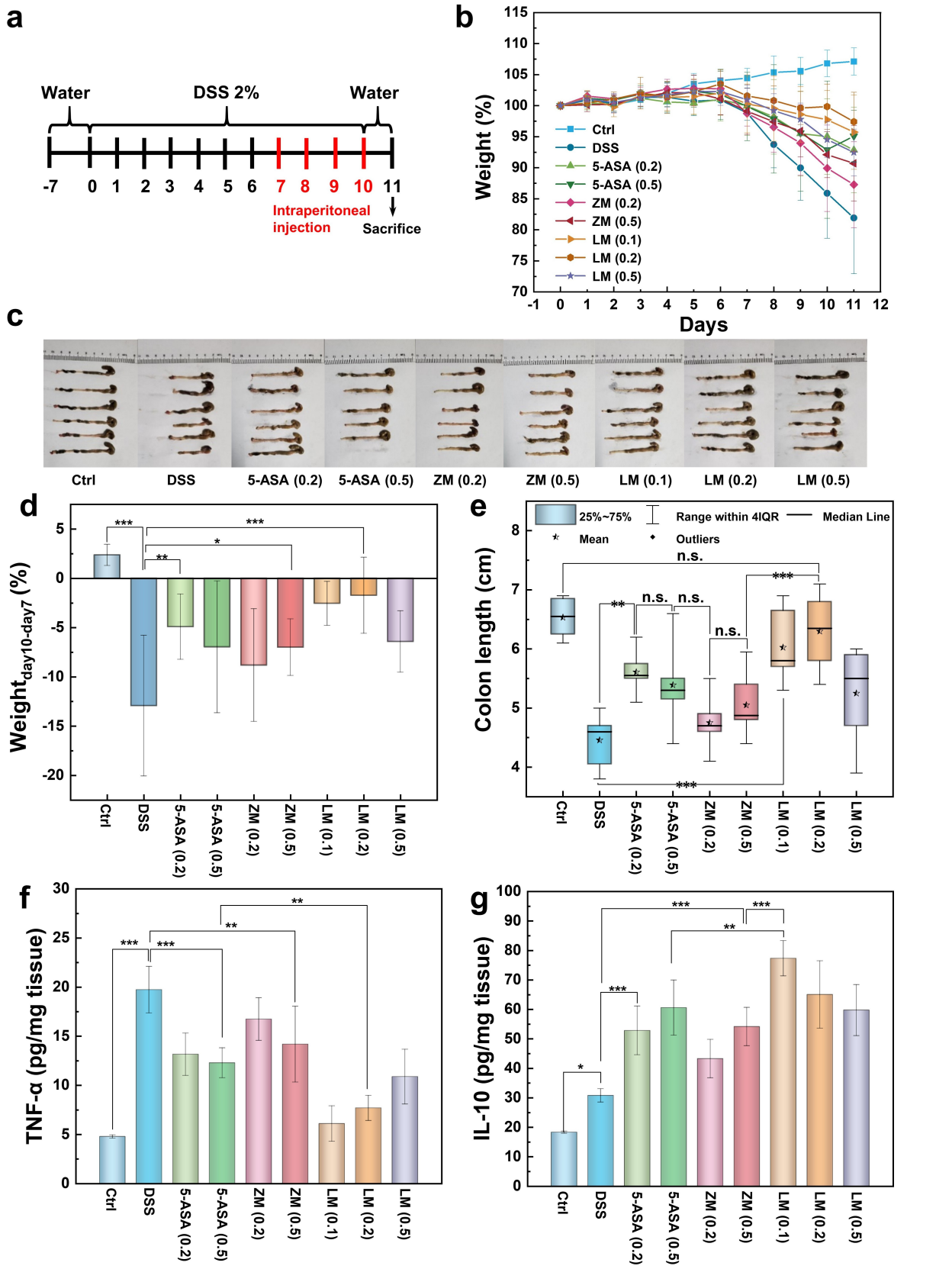

Figure 5. IBD therapy, tissue section and cytokine analysis. a) Overall process of animal experiment (DSS-induced colitis). b) Daily weight development in 11 days. c) The images of the colons and e) the statistics of the corresponding colon lengths in indicated groups. d) Changes in body weight of mice before (day 7) and after (day 10) treatments. Notably, one mouse died in the 5-ASA (0.5) group. The data are shown as mean ± SD ($n = 6$). * $P < 0.05$, ** $P < 0.01$ and *** $P < 0.005$; ns, not significant; t test. The expression levels of f) TNF-α and g) IL-10 in colon homogenate of each group. The data are shown as mean ± SD ($n = 4$).

acid (5-ASA), a medical drug for the treatment of IBD, were included as comparisons.

Figure 5a summarized the entire experimental procedure. After adaptive feeding, 2 wt % DSS was used to induce IBD in mice for ten consecutive days (day 0 to day 10). The weight loss on day 7 of all DSS-induced groups indicated the successful onset of IBD. Then, each mouse was intraperitoneally injected with different doses of LM, ZM and 5-ASA for four consecutive days (days 7, 8, 9, and 10) (Figure 5b). For simplification, the dosage such as $0.2\,mg\,kg^{-1}$ ZM was abbreviated as ZM (0.2), and other dosages were written in the same way. After that, the colon was photographed after the mice were sacrificed on day 11 (Figure 5c). The statistical results of colon length revealed the following information: first, LM, ZM, and 5-ASA all exhibited the therapeutic effects; second, the therapeutic efficacies of ZM and 5-ASA were close and did not show an obvious concentration dependence; and third, LM exhibited the most superior therapeutic efficacy and had a dose advantage, especially at a dose of $0.1\,mg\,kg^{-1}$. This was attributed to its excellent multiple antioxidant properties. The decrease in the therapeutic efficacy at a dose of $0.5\,mg\,kg^{-1}$ may be caused by its potential toxicity (Figure 5e). The weight change data of mice also showed a similar trend (Figure 5d), i.e., the doses of $0.2\,mg\,kg^{-1}$ and $0.1\,mg\,kg^{-1}$ LM significantly alleviated the symptoms of IBD.

Through histological staining of colon sections, we once again observed similar treatment effects and differences between groups with colon length and weight change data (Figure S16). Furthermore, the cytokine level was detected oin the homogenate of colon tissue. Nanozymes effectively down-regulated the pro-inflammatory factor TNF-α and up-regulated the anti-inflammatory factor IL-10, and the overall regulation is consistent with their therapeutic effects (Figure 5f and Figure 5g). Consistent with the trends of multiple antioxidant activities, the animal inflammation model clarified the application advantages of self-cascading antioxidant nanozyme (LM) against the diverse ROS environment from many aspects. The *in vivo* toxicity of nanozymes to the main organs (heart, liver, spleen, lung, and kidney) was also evaluated through pathological observation, and none of the experimental groups showed obvious toxicity (Figure S17).

Conclusion

Through the valence-engineered strategy, we demonstrated a case of regulating the multiple antioxidant activities of nanozymes. For the model material ZM, we found that with the incorporation of Li, the SOD-like, CAT-like and GPx-like activities of nanozymes were improved simultaneously. This is the first example of a positive correlation between multiple enzyme-like catalytic activities. In addition, the key factor that affects the enzymes-like activities has been elucidated, showing that valence of Mn significantly affected the activity of nanozymes. LM, as the finally optimized nanozyme, showed excellent performance in SOD-like, CAT-like and GPx-like activities, and had the ability to scavenge hydroxyl radicals. Its multiple antioxidant activity was verified in both cell and treatment of IBD. Especially in the treatment of IBD, there was a clear advantage in the therapeutic dose. This work not only has guiding significance for the development of nanozymes with multiple antioxidant activities, but also proves that the increase in activity and self-cascading construction can reduce the doses of therapeutic nanozymes, which will broaden the potential of nanozymes in biomedical applications.

Acknowledgements

We thank Prof. Rong Li for sharing the details of the SOD-like activity test. Funding: This work was supported by the National Key R&D Program of China (2019YFA0709200 and 2021YFF1200700), the Innovation Foundation of Nanjing University, National Natural Science Foundation of China (21874067 and 21722503), PAPD Program, Fundamental Research Funds for the Central Universities (021314380195), and Interdisciplinary Project Funded by Graduate School of Nanjing University (2018CL13).

Conflict of Interest

The authors declare no conflict of interest.

Data Availability Statement

The data that support the findings of this study are available from the corresponding author upon reasonable request.

Keywords: Antioxidant · Reactive Oxygen Species · Self-Cascade Nanozyme · Spinel Oxide · Valence-Engineering Strategy

[1] B. Yang, Y. Chen, J. Shi, *Chem. Rev.* **2019**, *119*, 4881–4985.
[2] a) D. Trachootham, J. Alexandre, P. Huang, *Nat. Rev. Drug Discovery* **2009**, *8*, 579–591; b) K. J. Barnham, C. L. Masters, A. I. Bush, *Nat. Rev. Drug Discovery* **2004**, *3*, 205–214; c) P. Fraisl, J. Aragones, P. Carmeliet, *Nat. Rev. Drug Discovery* **2009**, *8*, 139–152.
[3] a) X. Huang, X. Liu, Q. Luo, J. Liu, J. Shen, *Chem. Soc. Rev.* **2011**, *40*, 1171–1184; b) G. Mugesh, W.-W. du Mont, H. Sies, *Chem. Rev.* **2001**, *101*, 2125–2180; c) D. P. Riley, *Chem. Rev.* **1999**, *99*, 2573–2587; d) Z. Dong, J. Liu, S. Mao, X. Huang, B. Yang, X. Ren, G. Luo, J. Shen, *J. Am. Chem. Soc.* **2004**, *126*, 16395–16404; e) S. Yu, Y. Yin, J. Zhu, X. Huang, Q. Luo, J. Xu, J. Shen, J. Liu, *Soft Matter* **2010**, *6*, 5342–5350.
[4] a) H. Wei, E. Wang, *Chem. Soc. Rev.* **2013**, *42*, 6060–6093; b) J. Wu, X. Wang, Q. Wang, Z. Lou, S. Li, Y. Zhu, L. Qin, H. Wei, *Chem. Soc. Rev.* **2019**, *48*, 1004–1076; c) Y. Huang, J. Ren, X. Qu, *Chem. Rev.* **2019**, *119*, 4357–4412; d) H. Wei, L. Gao, K. Fan, J. Liu, J. He, X. Qu, S. Dong, E. Wang, X. Yan, *Nano Today* **2021**, *40*, 101269; e) M. Liang, X. Yan, *Acc. Chem. Res.* **2019**, *52*, 2190–2200; f) R. Zhang, X. Yan, K. Fan, *Acc. Mater. Res.* **2021**, *2*, 534–547; g) X. Zhang, R. Huang, S. Gopalakrishnan, R. Cao-Milán, V. M. Rotello, *Trends Chem.* **2019**, *1*,

90–98; h) K. Korschelt, M. N. Tahir, W. Tremel, *Chem. Eur. J.* **2018**, *24*, 9703–9713; i) F. Mancin, L. J. Prins, P. Pengo, L. Pasquato, P. Tecilla, P. Scrimin, *Molecules* **2016**, *21*, 1014; j) H. Dong, Y. Fan, W. Zhang, N. Gu, Y. Zhang, *Bioconjugate Chem.* **2019**, *30*, 1273–1296.

[5] a) J. Wu, Y. Yu, Y. Cheng, C. Cheng, Y. Zhang, B. Jiang, X. Zhao, L. Miao, H. Wei, *Angew. Chem. Int. Ed.* **2021**, *60*, 1227–1234; *Angew. Chem.* **2021**, *133*, 1247–1254; b) M. Chang, Z. Hou, M. Wang, M. Wang, P. Dang, J. Liu, M. Shu, B. Ding, A. A. Al Kheraif, C. Li, J. Lin, *Small* **2020**, *16*, 1907146; c) Y. Yang, M. Chen, B. Wang, P. Wang, Y. Liu, Y. Zhao, K. Li, G. Song, X. B. Zhang, W. Tan, *Angew. Chem. Int. Ed.* **2019**, *58*, 15069–15075; *Angew. Chem.* **2019**, *131*, 15213–15219; d) G. Wu, V. Berka, P. J. Derry, K. Mendoza, E. Kakadiaris, T. Roy, T. A. Kent, J. M. Tour, A.-L. Tsai, *ACS Nano* **2019**, *13*, 11203–11213; e) D. Wang, H. Wu, W. Q. Lim, S. Z. F. Phua, P. Xu, Q. Chen, Z. Guo, Y. Zhao, *Adv. Mater.* **2019**, *31*, 1901893.

[6] a) Z. Wang, X. Shen, X. Gao, Y. Zhao, *Nanoscale* **2019**, *11*, 13289–13299; b) V. Patel, M. Singh, E. L. Mayes, A. Martinez, V. Shutthanandan, V. Bansal, S. Singh, A. S. Karakoti, *Chem. Commun.* **2018**, *54*, 13973–13976; c) C. Korsvik, S. Patil, S. Seal, W. T. Self, *Chem. Commun.* **2007**, 1056–1058; d) V. Baldim, F. Bedioui, N. Mignet, I. Margaill, J.-F. Berret, *Nanoscale* **2018**, *10*, 6971–6980.

[7] a) H. Cheng, L. Zhang, J. He, W. Guo, Z. Zhou, X. Zhang, S. Nie, H. Wei, *Anal. Chem.* **2016**, *88*, 5489–5497; b) X. Cai, L. Jiao, H. Yan, Y. Wu, W. Gu, D. Du, Y. Lin, C. Zhu, *Mater. Today* **2021**, *44*, 211–228.

[8] a) A. Adhikari, S. Mondal, M. Das, P. Biswas, U. Pal, S. Darbar, S. S. Bhattacharya, D. Pal, T. Saha-Dasgupta, A. K. Das, A. K. Mallick, S. K. Pal, *Adv. Healthc. Mater.* **2021**, *10*, 2001736; b) Y. Liu, Y. Cheng, H. Zhang, M. Zhou, Y. Yu, S. Lin, B. Jiang, X. Zhao, L. Miao, C.-W. Wei, *Sci. Adv.* **2020**, *6*, eabb2695; c) Y. Y. Huang, Z. Liu, C. Q. Liu, E. G. Ju, Y. Zhang, J. S. Ren, X. G. Qu, *Angew. Chem. Int. Ed.* **2016**, *55*, 6646–6650; *Angew. Chem.* **2016**, *128*, 6758–6762.

[9] a) T. Chen, H. Zou, X. Wu, Y. Chen, B. Situ, L. Zheng, G. Yang, *ACS Biomater. Sci. Eng.* **2019**, *5*, 3079–3088; b) X. Zhang, S. Zhang, Z. Yang, Z. Wang, X. Tian, R. Zhou, *Nanoscale* **2021**, *13*, 12613–12622.

[10] Q. Zhao, Z. Yan, C. Chen, J. Chen, *Chem. Rev.* **2017**, *117*, 10121–10211.

[11] a) Y. Zhou, S. Sun, J. Song, S. Xi, B. Chen, Y. Du, A. C. Fisher, F. Cheng, X. Wang, H. Zhang, Z. J. Xu, *Adv. Mater.* **2018**, *30*, 1802912; b) Y. Zhou, S. Sun, C. Wei, Y. Sun, P. Xi, Z. Feng, Z. J. Xu, *Adv. Mater.* **2019**, *31*, 1902509; c) J. Yao, Y. Cheng, M. Zhou, S. Zhao, S. Lin, X. Wang, J. Wu, S. Li, H. Wei, *Chem. Sci.* **2018**, *9*, 2927–2933; d) N. Singh, M. A. Savanur, S. Srivastava, P. D′Silva, G. Mugesh, *Angew. Chem. Int. Ed.* **2017**, *56*, 14267–14271; *Angew. Chem.* **2017**, *129*, 14455–14459.

[12] Y. Lee, K. Sugihara, M. G. Gillilland III, S. Jon, N. Kamada, J. J. Moon, *Nat. Mater.* **2020**, *19*, 118–126.

[13] S. Zhao, Y. Li, Q. Liu, S. Li, Y. Cheng, C. Cheng, Z. Sun, Y. Du, C. J. Butch, H. Wei, *Adv. Funct. Mater.* **2020**, *30*, 2004692.

[14] a) M. Chen, R. Wu, S. Ju, X. Zhang, F. Xue, W. Xing, *Microporous Mesoporous Mater.* **2018**, *261*, 29–34; b) Q. Jiang, D. Liu, H. Zhang, S. Wang, *J. Phys. Chem. C* **2015**, *119*, 28776–28782; c) Z. Y. Guo, C. X. Li, M. Gao, X. Han, Y. J. Zhang, W. J. Zhang, W. W. Li, *Angew. Chem. Int. Ed.* **2021**, *60*, 274–280; *Angew. Chem.* **2021**, *133*, 278–284; d) J. Y. Piao, S. Y. Duan, X. J. Lin, X. S. Tao, Y. S. Xu, A. M. Cao, L. J. Wan, *Chem. Commun.* **2018**, *54*, 5326–5329.

[15] T. Lin, X. Zhao, S. Zhao, H. Yu, W. Cao, W. Chen, H. Wei, H. Guo, *Theranostics* **2018**, *8*, 990–1004.

Manuscript received: January 20, 2022
Accepted manuscript online: April 22, 2022
Version of record online: May 5, 2022